tures are reported with a hexagonal subcell. Probably distortion of the tellurium lattice becomes too large to be realized by an incommensurable modulation.

Concluding remarks

The average orthorhombic phase of $Cu_{3-x}Te_2$ is analogous to that of $Ni_{3\pm x}Te_2$ and has a close packing of Te atoms in which partially occupied Cu^{II} sites become ordered along the *a* direction (still random along *b*). The Te—Te distances indicate that, unlike in the nickel compound, there is considerable charge transfer from the Cu to the Te atoms. This is reflected in the modulation: the Te atoms are strongly displaced towards the empty Cu^{II} sites. The displacements of the Cu^{I} atoms follow the tellurium lattice. The ordering of the Cu^{II} sites along *a* (Fig. 1) is described by the modulation wavevector $\mathbf{q} = 0.397\mathbf{a}^* + \frac{1}{2}\mathbf{c}^*$, incommensurable with the basic lattice. The ordering is determined quantitatively with first- and second-order harmonics of the modulation wave; probably higher-order harmonics should be used for a more precise description. The representation of the occupation modulation with a shear-structure-like model is possible. An explanation of the origin of the incommensurable modulation can be given in terms of two competing interactions, between the ordering of the Cu^{II} sites and the polarizability of the Te lattice. The difference between this case and the nickel telluride originates from a different interaction strength and a different charge transfer between the metal atom and Te. The homogenity range of the modulated phase seems to be much smaller (somewhere around $x = 0.11$) than was previously proposed, as we found only small differences in the modulation (including occupation) parameters for two samples prepared under rather different conditions ($x = 0.26$ and $x = 0.02$).

This work is part of the research program of the Netherlands Foundation for Chemical Research (SON) and was made possible by financial support from the Netherlands Organisations for Scientific Research (NWO).

References

ANDERKO, K. & SCHUBERT, K. (1954). *Z. Metallkd.* **45**, 371.
BARANOVA, R. V. & PINSKER, Z. G. (1964). *Sov. Phys. Crystallogr.* **9**, 83.
BOER, J. L. DE & DUISENBERG, A. J. M. (1984). Enraf–Nonius CAD-4F diffractometer software. Groningen and Utrecht, The Netherlands.
COLAITIS, D., DELAVIGNETTE, P., VAN DYCK, D. & AMELINCKX, S. (1979). *Phys. Status Solidi A*, **51**, 657–672.
COLAITIS, D., VAN DYCK, D., DELAVIGNETTE, P. & AMELINCKX, S. (1979). *Phys. Status Solidi A*, **53**, 423–431.
COLAITIS, D., VAN DYCK, D., DELAVIGNETTE, P. & AMELINCKX, S. (1980). *Phys. Status Solidi A*, **58**, 271–288.
DYCK, D. VAN, COLAITIS, D., DELAVIGNETTE, P. & AMELINCKX, S. (1979). *Phys. Status Solidi A*, **53**, 105–112.
FORMAN, S. & PEACOCK, M. A. (1949). *Am. Mineral.* **34**, 441.
JANNER, A., JANSSEN, T. & DE WOLFF, P. M. (1983). *Acta Cryst.* A**39**, 671–678.
JELLINEK, F. (1972). *MTP International Review of Science, Inorganic Chemistry*, Series 1, Vol. 5. London: Butterworth.
SCHUTTE, W. J. & DE BOER, J. L. (1993). *Acta Cryst.* B**49**, 392–398.
STEVELS, A. L. N. (1969). *Philips Res. Rep. Suppl.* **9**, 1–128.
WOLFF, P. M. DE (1974). *Acta Cryst.* A**30**, 777–785.
WOLFF, P. M. DE, JANSSEN, T. & JANNER, A. (1981). *Acta Cryst.* A**37**, 625–636.
YAMAMOTO, A. (1982). *Acta Cryst.* A**38**, 87–92.
YAMAMOTO, A. (1985). *REMOS*85.0. Program for the refinement of modulated structures. National Institute for Research in Inorganic Materials, Sakura-Mura, Niihari-Gun, Ibaraki 305, Japan.

Acta Cryst. (1993). B**49**, 403–413

Neutron Powder Investigation of Tetragonal and Cubic Stabilized Zirconia, TZP and CSZ, at Temperatures up to 1400 K

BY U. MARTIN, H. BOYSEN AND F. FREY

Institut für Kristallographie und Mineralogie der Universität, Theresienstrasse 41, 8000 *München* 2, *Germany*

(*Received* 12 *June* 1992; *accepted* 22 *October* 1992)

Abstract

A comparative study of tetragonal (Y-TZP, 3 mol% Y_2O_3) and cubic (CSZ, 15 mol% CaO) zirconia powder samples was carried out to learn about a possible structural origin of the superior ionic conductivity of TZP at low temperatures. Structure refinements including anharmonic temperature factors and oxygen occupancies as well as a qualitative analysis of the diffuse background revealed large differences especially of the anisotropy of thermal motion and the underlying disorder in both samples.

0108-7681/93/030403-11$06.00

Diffusion pathways are restricted to layers in TZP, in contrast with a three-dimensional behaviour in CSZ. The structural arrangement of the tetragonal phase is slightly more favourable for conduction processes. More importantly, the higher concentration of oxygen vacancies in CSZ is less operative due to an immobilization of these charge carriers by coherent and incoherent microclustering at low temperatures, whereas the smaller number of vacancies in TZP is fully available for transport processes. At higher temperatures – as CSZ approaches the true thermodynamic stability field of the cubic structure – the stabilizing function of the microclusters decreases, the clusters dissolve and the ionic conductivity in CSZ becomes superior to that in TZP. No such processes take place in TZP. The behaviour in powdered samples differs from that in single crystals.

1. Introduction

Zirconia, ZrO_2, doped with aliovalent oxides like CaO, Y_2O_3 or MgO, is of outstanding interest in materials science due to the intimate relation between its structural and physical properties. At ambient pressure, pure zirconium dioxide exists in three basic polymorphs: cubic (*Fm3m*, fluorite) and tetragonal ($P4_2/nmc$, distorted fluorite) high-temperature phases, and a monoclinic ($P2_1/c$) phase stable at room temperature. Depending on several factors such as composition, grain size and material processing, the tetragonal or the cubic structure can be retained at ambient temperature. A schematic picture of the structural relationship between these phases is given in Fig. 1.

The so-called tetragonal zirconia polycrystal (TZP) has excellent room-temperature mechanical properties (for a review see Nettleship & Stevens, 1987) and an enhanced ionic conductivity at low temperatures as compared with cubic zirconia, *e.g.* CSZ (calcia-stabilized zirconia) (Bonanos, Slotwinski, Steele & Butler, 1984; Weppner & Schubert, 1988; Turrillas, Sellars & Steele, 1988), despite the lower vacancy concentration (1.5% in TZP and 7.5% in CSZ in the samples investigated here). The stability of tetragonal zirconia (Mitsuhashi, Ichihara & Tatsuke, 1974) and the enhanced fracture toughness (Michel, Mazerolles & Perez y Jorba, 1983) were discussed in terms of domain structures. It is not clear, however, whether the tetragonality itself, the defect structure or the microstructure of TZP are most decisive for the enhanced ionic conductivity. With this work we intend to clarify whether the structural differences between the cubic fluorite structure and its slightly distorted tetragonal modification and the defect/domain structures might be responsible for the different ionic conductivities and other material properties.

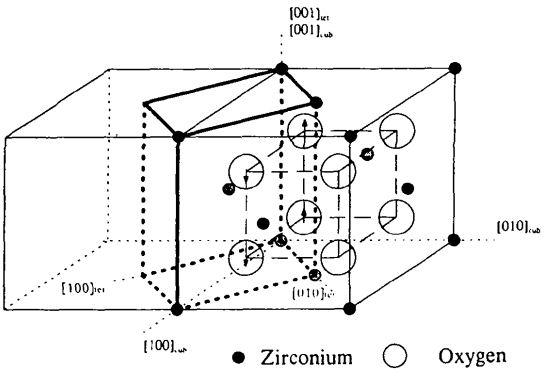

Fig. 1. Relationships between the unit cells of the tetragonal and cubic structures of zirconia.

Most of the previous studies were performed on quenched and annealed samples; no high-temperature investigations have been reported for TZP. Therefore, many structural questions remain open, as the following examples illustrate.

(i) Are there structural differences between the real equilibrium phases at high temperatures and the quenched phases at lower temperatures? From the phase diagrams these stability fields exist above 1200 K in the ZrO_2–CaO system (Stubican, 1988) and 800 K in the ZrO_2–Y_2O_3 system (Scott, 1975).

(ii) The defect structure of CSZ is not fully understood and is still a subject of controversy in the literature: Neder, Frey & Schulz (1990) and Proffen, Neder, Frey, Keen & Zeyen (1993) interpreted the diffuse scattering observed with neutrons in single crystals by two types of coherent correlated microclusters, while Rossel, Sellar & Wilson (1991) deduced coherently intergrown microdomains of the so-called Φ_1 type from their electron-microscope studies. This latter phase, $CaZr_4O_9$, emerges after long annealing of bulk crystals or sintered material at high temperatures. An analysis of the averaged structure of CSZ (15 mol% CaO) at high temperatures (Lorenz, Frey, Schulz & Boysen, 1988) clearly shows a superposition of static and dynamic disordering.

(iii) Are there indications for microdomains in TZP too and, if so, are these domains coherent or incoherent? It may be worth recalling that any kind of static or dynamic disorder, *i.e.* deviation from a strictly periodic arrangement of the atoms, gives rise to diffuse scattering. This includes statistical disorder (positional, occupational), short-range order, microdomains or clusters, segregations, amorphous regions *etc.* In the case of coherence with the lattice of the surrounding crystalline matrix, this disorder is also found in the average structure, which is obtained by projecting the contents of all individual unit cells into a single unit cell and which can be determined from an analysis of the Bragg reflexions

alone. On the other hand, incoherent segregations give rise to diffuse scattering only.

(iv) Concerning the concentration and distribution of oxygen vacancies: are they responsible for the enhanced low-temperature conductivity and how do they influence the defect structure?

Crystal structure determinations on tetragonal (undoped) ZrO_2 have been performed using X-ray and neutron powder diffraction between 1470 and 2230 K by Teufer (1962) and between 1100 and 1900 K by Frey, Boysen & Vogt (1990) and Boysen, Frey & Vogt (1991), respectively. Further structure investigations of yttria-stabilized TZP (Y-TZP) were carried out at room temperature by Michel *et al.* (1983) using X-ray powder diffraction and by Howard, Hill & Reichert (1988) using neutron powder diffraction. CSZ samples have been analysed from both X-ray and neutron data at various temperatures by Carter & Roth (1968), Faber, Müller & Cooper (1978), Morinaga, Cohen & Faber (1979), Lorenz *et al.* (1988) and Neder *et al.* (1990).

2. Experiments and data analysis

The stabilization of tetragonal zirconia depends on factors such as grain size, composition, density and firing treatment. Single-phase tetragonal material is obtained only under well defined preparation conditions. The pure tetragonal polycrystalline zirconia crystals used here were two specimens containing 3.0 and 2.5 mol% Y_2O_3 as stabilizer (provided by MPI-Stuttgart). They were made by pressing the powder into the desired shape and size for neutron diffraction (a cylinder of diameter 1 cm) followed by sintering for 2 h at 1400 K. The pure tetragonal phase is only obtained within the concentration limits of 2.5–3.0 mol% Y_2O_3. Since the two samples showed no significant differences, only the one with 3 mol% stabilizer is described in the following. The cubic specimen was prepared by grinding a single crystal with 15 mol% CaO, grown by the skull method (provided by Djevahirdjan Company, Switzerland).

Diffraction data of all samples were collected on the neutron powder diffractometer MAN I at the reactor facility FRM in Garching, Germany. The high-temperature scattering furnace has a niobium heating element and provides temperatures up to 1400 K with a stability of $\Delta T = \pm 1$ K. The specimens were contained in a niobium can. Measurements were made between room temperature (r.t.) and 1400 K for TZP and at r.t. and 770 K for CSZ. The data were recorded under monitor control at intervals of $\Delta(2\theta) = 0.1°$ over an angular range $2\theta \leq 104°$, with a wavelength of $\lambda = 1.075$ Å. The scattering lengths used for Zr, Ca, Y and O were 7.16, 4.9, 7.75 and 5.805 fm, respectively. The least-squares structure refinements were performed with the Rietveld-program version of Thomas & Bendall (1978), extended for anharmonic temperature factors by Boysen (1992). Further data evaluation (probability density function maps, potentials) was performed with the (single-crystal) program system *PROMETHEUS* (Zucker, Perenthaler, Kuhs, Bachmann & Schulz, 1983). For a discussion of the significance of anharmonic thermal parameters from powder patterns, see Boysen (1992). The strong modulated background was defined manually. Nb was treated as a second phase during the fits and has poor agreement, as shown by the deviations in the difference plots in Fig. 2. Gaussian profile functions that best represent the actual instrumental resolution function of the diffractometer were employed throughout. Examples of observed and calculated neutron powder diffraction patterns and their difference curves are given in Fig. 2.*

In this work, essential information is drawn from a temperature-factor analysis of the Bragg data. Generally, the temperature factor $T(\mathbf{h})$ is the Fourier transform of the probability density function p.d.f.($\mathbf{u}$), which describes the space- and time-averaged distribution of the displacements $\mathbf{u} = \mathbf{x} - \mathbf{x}_j$ of the atoms around their equilibrium positions $\mathbf{x}_j$,

$$T_j(\mathbf{h}) = \int \text{p.d.f.}_j(\mathbf{u}) \exp(2\pi i \mathbf{h}\cdot\mathbf{u}) \, \mathrm{d}V. \qquad (1)$$

This relation holds both for dynamic and static disorder. Note that the usual 'harmonic' temperature factor corresponds to a Gaussian p.d.f. With the assumption that the thermal motion (oscillations, diffusion, *etc.*) of the atoms in a single-particle potential $V(\mathbf{u})$ is independent (an approximation that is valid at high temperatures), Boltzmann statistics give

$$\text{p.d.f.}_j(\mathbf{u}) = \exp[-V_j(\mathbf{u})/kT] \text{p.d.f.}_j(\mathbf{0}). \qquad (2)$$

Significantly anharmonic p.d.f.'s and temperature factors are encountered in the case of large atomic motions, particularly at high temperatures. A possible approximation is given by the Gram–Charlier expansion (Johnson & Levy, 1974),

$$T_j(\mathbf{h}) = T_{j/\text{harmon}}(\mathbf{h})\{1 + [(2\pi i)^3/3!] c_j^{pqr} h_p h_q h_r + [(2\pi i)^4/4!] d_j^{pqrs} h_p h_q h_r h_s + \ldots\}, \qquad (3)$$

where c_j^{pqr} and d_j^{pqrs} are the refinable coefficients of third and fourth order, respectively. For more details, see, for example, Zucker *et al.* (1983).

For static disordered structures the average distribution of the displacements may be approximated by the same formalism, although the Gram–Charlier expansion is not always the most suitable. Of course,

* Primary diffraction data have been deposited with the British Library Document Supply Centre as Supplementary Publication No. SUP 55965 (38 pp.). Copies may be obtained through The Technical Editor, International Union of Crystallography, 5 Abbey Square, Chester CH1 2HU, England.

the derivation of a potential, V, makes no sense in this case. A separation of static and dynamic contributions to the temperature factor may be attained by analysis of its temperature dependence: in the purely dynamic case and in the harmonic approximation, the thermal displacement parameters should be proportional to the temperature, *i.e.* they should extrapolate to zero at 0 K. Hence, a positive finite value obtained from an extrapolation to 0 K may be attributed to static disorder. This argument is not true at very low temperatures ($T < \Theta_{Debye}$), where quantum effects (zero-point motion) come into play. At too high temperatures, anharmonicity leads to a steeper increase with temperature and, in the absence of static disorder, would lead to negative values at 0 K. Similar extrapolations are possible for the higher-order terms. This widely used procedure is, however, subject to some uncertainties (possible temperature dependence of the static disorder, anharmonicity at high temperatures). Instead, more reliable conclusions may be drawn from the temperature dependence of the derived potentials (Bachmann & Schulz, 1984), which should be practically independent of temperature in the purely dynamic case. The dependence will become steeper with increasing temperature in the presence of static contributions because the relative amount of the latter becomes less important compared with thermal motion.*

Table 1. *Final parameters of TZP*

(*a*) Harmonic refinements

	295 K	570 K	770 K	1060 K	1200 K	1400 K
z(O)	0.4589 (4)	0.4578 (3)	0.4570 (3)	0.4563 (4)	0.4557 (4)	0.4553 (4)
β_{11}(O)	0.020 (2)	0.036 (2)	0.045 (2)	0.053 (3)	0.067 (3)	0.076 (3)
β_{22}(O)	0.010 (2)	0.021 (2)	0.023 (2)	0.026 (2)	0.025 (2)	0.033 (2)
β_{33}(O)	0.0076 (6)	0.0115 (5)	0.0149 (5)	0.0181 (7)	0.0207 (8)	0.0234 (9)
B(Zr) (Å^2)	0.37 (4)	0.72 (3)	0.98 (3)	1.19 (4)	1.40 (4)	1.65 (4)
n(O)	1.95 (2)	1.99 (2)	1.97 (1)	1.97 (2)	1.98 (2)	1.96 (2)
a (Å)	3.6067 (4)	3.6136 (3)	3.6227 (3)	3.6359 (4)	3.6411 (4)	3.6498 (4)
c (Å)	5.1758 (8)	5.1909 (5)	5.2056 (5)	5.2257 (7)	5.2341 (7)	5.2481 (8)
R_{exp} (%)	10.60	7.46	5.78	6.26	5.04	6.67
R_{wp} (%)	14.03	10.90	10.33	11.71	11.59	11.97
R_I (%)	3.53	4.66	3.34	5.70	5.02	5.65

(*b*) Anharmonic refinements

	770 K	1060 K	1200 K	1400 K
z(O)	0.4566 (4)	0.4558 (5)	0.4549 (5)	0.4549 (6)
β_{11}(O)	0.043 (2)	0.051 (3)	0.064 (3)	0.071 (3)
β_{22}(O)	0.024 (2)	0.027 (3)	0.027 (2)	0.037 (2)
β_{33}(O)	0.0149 (5)	0.0182 (7)	0.0208 (8)	0.0235 (8)
$c^{333} \times 10^3$	–	–	–	0.014 (8)
$c^{111} \times 10^3$	−0.010 (6)	−0.014 (9)	−0.026 (11)	−0.040 (12)
B(Zr) (Å^2)	0.99 (3)	1.20 (4)	1.42 (4)	1.68 (5)
n(O)	1.96 (1)	1.97 (2)	1.98 (2)	1.96 (2)
a (Å)	3.6227 (3)	3.6358 (4)	3.6411 (4)	3.6499 (4)
c (Å)	5.2056 (6)	5.2257 (7)	5.2340 (7)	5.2483 (8)
R_{exp} (%)	5.78	6.25	5.04	6.65
R_{wp} (%)	10.31	11.69	11.55	11.84
R_I (%)	3.28	5.67	4.73	5.49

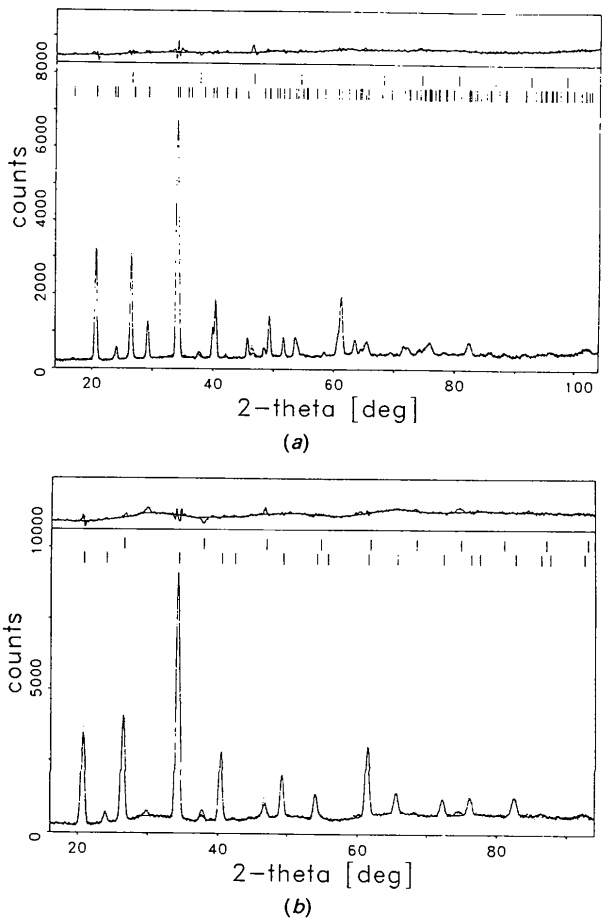

Fig. 2. Observed (dots) and calculated (solid line) neutron powder patterns of (*a*) TZP (3 mol% Y_2O_3) at 1400 K and (*b*) CSZ (15 mol% CaO) at 770 K. Difference plots with a manually defined background are shown at the top to the same scale. Upper marks correspond to Nb, lower ones to zirconia.

3. Results

TZP

To analyse the temperature dependence of the structural parameters of $Zr_{0.94}Y_{0.06}O_{1.97}$, refinements up to 1400 K were carried out in space group $P4_2/nmc$ (origin at centre of symmetry) with the Zr and O atoms in special positions 2(*a*) and 4(*d*), respectively. Several models were examined, including harmonic and anharmonic temperature factors for O and harmonic ones for Zr. The latter turned out to be isotropic in all cases. The thermal displacement parameters were refined together with lattice constants, the positional O parameter z(O) and, as an important extension of former analyses, the site occupancy of the O atoms n(O). The refined parameters are presented in Table 1.

* To stress the applicability of (harmonic or anharmonic) temperature factors to both static and dynamic disorder, the term 'atomic displacement parameters' instead of 'thermal displacement parameters' has been advocated in the literature (see, for example, Kuhs, 1992). However, to avoid confusion with the displacement of the equilibrium position of an atom (*e.g.* with temperature or during a phase transition) we will continue to use 'thermal' (mean-square) displacement parameters in the following.

The temperature dependence of the lattice constants shows no deviation from a linear behaviour. The O site occupancy was constant for all temperatures, $n(O) \simeq 1.97$ (2), in agreement with the stoichiometric ratio (charge balance). The value of $z(O)$ at r.t. is close to that of former investigations on the same material (Michel *et al.*, 1983; Howard *et al.*, 1988). It decreases slightly with increasing temperature. Together with a slight increase of the *c*:*a* ratio, this means an increase of the 'tetragonality'. The same tendency was found for pure ZrO_2 (Boysen *et al.*, 1991), however, with lower $z(O)$ values ($\Delta z \simeq 0.008$) and larger *c*:*a* ratios (by about 0.8%). Therefore, TZP is less 'tetragonal' than pure *t*-ZrO_2.

It should be mentioned that a slight increase of the linewidths with temperature was observed. A rough analysis in terms of particle sizes and strains gave no clear result. Instead, a fit with an additional cubic phase with a phase amount of up to 8% at the highest temperature was possible, yielding slightly improved *R* factors, 'normal' half-width parameters and practically no change of the parameters of the tetragonal phase. The error bars for the parameters of the cubic phase were, however, so large that no definite conclusions may be drawn with the present resolution of the instrument. Such a cubic component would, however, be compatible with the phase diagram (Scott, 1975).

The extrapolation of the harmonic B_{ij} ($=8\pi^2\langle u^2_{ij}\rangle$) values to 0 K (Fig. 3) shows small static contributions for O between 0.10 and 0.35 Å^2, but almost none for Zr. There is a significant anisotropy: $B_{11} > B_{33} > B_{22}$. Since the static part is not very different for the three components, the anisotropy is mainly due to dynamic effects. The same anisotropy was found for *t*-ZrO_2 (Boysen *et al.*, 1991) and was explained by shallow potentials in connection with the $t \rightarrow m$ phase transformation. However, together with the third-order terms of the temperature factor, they may be indicative of possible diffusion pathways as discussed below. Out of the three symmetry-allowed third-order coefficients c^{333}, c^{113} and c^{223}, only c^{113} becomes significant above 700 K and c^{333} becomes significant at 1400 K. The corresponding p.d.f.s are discussed below.

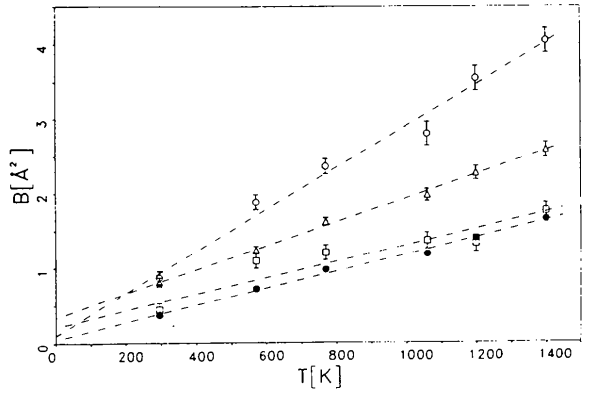

Fig. 3. Temperature dependence of the harmonic temperature factors of Zr (●, B_{iso}) and O (○, B_{11}; □, B_{22}; △, B_{33}) in TZP.

The background does not show strong modulations. Hence, there are no indications of any correlations, precipitations *etc.* It is, however, quite large, thus indicating statistical disorder (monotonic Laue scattering) – presumably statistical relaxations of the atoms around vacancies. This confirms the static contribution derived from the temperature-factor analysis above.

CSZ

Previous neutron measurements on the same material were carried out on single crystals at 1170, 1370 and 1570 K (Lorenz *et al.*, 1988) and on powder samples at 1300 and 1550 K (Marxreiter, 1989). This means that all experiments were carried out either at r.t. or in the high-temperature region, where cubic $Zr_{0.85}Ca_{0.15}O_{1.85}$ is close to or in its thermodynamic stability field. The aim of the present powder experiments at r.t. and 770 K was to check whether the disorder analysis performed previously for temperatures above 1200 K is also valid in the low-temperature regime (770 K). This point is of particular interest since static disorder phenomena like microclustering are assumed to be the limiting factor for the low-temperature conduction properties of this material (Neder *et al.*, 1990).

Refinements of the r.t. and 770 K measurements were performed first in space group *Fm*3*m* with the Zr and O atoms in special positions 4(*a*) and 8(*c*), respectively. Three cubic models were examined for the O atoms: harmonic (isotropic by symmetry) temperature factors, split positions along ⟨100⟩ [special positions 24(*e*)] and anharmonic temperature factors up to the fourth order. Refinement agreement (*R*) factors and results are presented in Table 2(*a*). It should be mentioned that a ⟨111⟩ split model as suggested by Carter & Roth (1968) for zirconia of the same composition has also been tried. Their value of the *x* parameter (0.277) is in remarkable agreement with the value found here (0.270). However, here the ⟨100⟩ model is clearly favoured by a better fit, in agreement with the findings of Faber *et al.* (1978), although their *x* parameter (0.206) is in disagreement with our results. The latter authors also report an increasing O order with annealing time, which they interpret as a tetragonal distortion of the lattice (see below).

Fig. 4 shows the *B* values as a function of temperature together with results of the high-temperature measurements of Lorenz *et al.* (1988) and Marxreiter (1989). In contrast with the con-

Table 2. *Final parameters of CSZ*

(*a*) Cubic refinements

	295 K			770 K		
	Harmonic	Split	Anharmonic	Harmonic	Split	Anharmonic
z(O)	0.25	0.237 (4)	0.25	0.25	0.224 (6)	0.25
β_{11}(O)	0.031 (1)	0.076 (9)	0.073 (5)	0.035 (1)	0.063 (12)	0.051 (6)
β_{22}(O)	-	0.022 (2)	-	-	0.023 (2)	-
β_{33}(O)	-	0.026 (6)	-	-	0.023 (6)	-
$c^{123} \times 10^3$	-	-	0.043 (9)	-	-	0.043 (7)
$d^{1111} \times 10^4$	-	-	0.37 (9)	-	-	0.11 (5)
$d^{1122} \times 10^4$	-	-	0.09 (2)	-	-	0.02 (1)
B(Zr) (Å^2)	1.17 (6)	1.24 (6)	1.30 (5)	1.79 (6)	1.89 (6)	1.93 (6)
n(O)	1.83 (3)	1.90 (3)	2.12 (4)	1.77 (2)	1.80 (3)	1.87 (5)
a (Å)	5.1289 (8)	5.1292 (8)	5.1291 (8)	5.1520 (8)	5.1523 (7)	5.1523 (7)
R_{exp} (%)	5.09	5.12	5.11	6.04	6.02	6.01
R_{wp} (%)	12.78	12.44	12.11	11.90	11.03	10.98
GOF$_{wp}$	2.51	2.43	2.37	1.97	1.84	1.82
R_I (%)	6.85	6.13	5.07	6.42	4.64	4.05

(*b*) Tetragonal refinements

	295 K		770 K	
	Anharmonic	Split	Anharmonic	Split
z(O)	0.462 (2)	0.5	0.470 (3)	0.5
β_{11}(O)	0.067 (7)	0.046 (3)	0.069 (7)	0.052 (4)
β_{22}(O)	0.114 (11)	-	0.111 (11)	-
β_{33}(O)	0.065 (4)	-	0.056 (6)	-
$c^{333} \times 10^3$	−0.58 (7)	-	−0.39 (9)	-
$c^{113} \times 10^3$	−0.17 (2)	-	−0.20 (2)	-
z(O′)	-	0.396 (14)	-	0.410 (19)
B(O′) (Å^2)	-	7.0 (1.3)	-	7.0 (1.6)
B(Zr) (Å^2)	1.32 (5)	1.25 (5)	1.96 (6)	1.85 (6)
n(O)	2.02 (3)	1.40 (7)	1.89 (3)	1.36 (9)
n(O′)	-	0.59 (7)	-	0.52 (10)
c (Å)	5.1290 (7)	5.1288 (7)	5.1523 (7)	5.1520 (8)
R_{exp} (%)	6.19	6.20	7.20	7.20
R_{wp} (%)	12.98	13.33	12.31	13.00
GOF$_{wp}$	2.10	2.15	1.71	1.81
R_I (%)	6.38	6.76	4.65	6.67

tinuous increase of B(Zr) the B(O) values show a bend in the temperature dependence, which does not occur for TZP (*cf.* Fig. 3). A crude extrapolation of the two points below 1100 K suggests a very large $B(O)_{stat} \simeq 3$ Å^2; for higher temperatures this part seems to decrease. Again, the static disorder is evidenced by the large diffuse background, which is, however, strongly modulated in this case, in contrast with TZP. These modulations indicate the strong correlations between the defects in CSZ.

The refinement with anharmonic terms up to the fourth order leads to a significant reduction of the R factors. This is, however, accompanied by an overoccupation of the anion sublattice of n(O) = 2.12 (4) for the r.t. measurement, whereas the 770 K refinement shows a value of n(O) = 1.87 (5) in agreement with the 'stoichiometric' value 1.85. An overoccupied anion substructure (or an underoccupation of the cation substructure?) seems, of course, to be unrealistic. We will consider below that this effect might be (partly) a consequence of an incoherent decomposition at lower temperatures. It should be admitted, however, that these results might also be an artefact of the refinement: a very complex disordered structure may be insufficiently described by the anharmonic expansion type used here (truncation effects!). To check this question further, the diffuse background of a powder pattern has to be analysed quantitatively.

It has been reported (Carter & Roth, 1968; Howard *et al.*, 1988) that diagrams of fine powders of cubic stabilized zirconia show an additional 'tetragonal' peak. It is an open question whether this peak is due to a strongly disordered tetragonal minority phase or due to slight tetragonal distortions of cubic zirconia itself. Both the r.t. and 770 K measurements show a broad maximum at the position of the forbidden 211_{cub} reflexion, which can also be identified as a superposition of the strongest tetragonal superlattice $201/102_{tet}$ reflexions. The enlarged plot shown in Fig. 5 demonstrates that this is really a peak on top of one of the broader diffuse humps of the background. Slightly enhanced intensity cannot be excluded at the positions of other strong tetragonal superlattice reflexions, although this can hardly be separated from the modulated background. Since the cubic reflexions show no line broadening with respect to instrumental resolution,

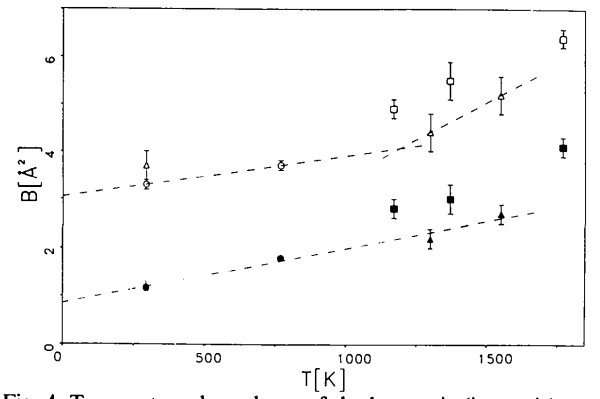

Fig. 4. Temperature dependence of the harmonic (isotropic) temperature factor of O in CSZ: (○) present work, (△) neutron powder (Marxreiter, 1989), (□) single crystal (Lorenz *et al.*, 1988), all carried out with same crystal material. Same for Zr: filled symbols.

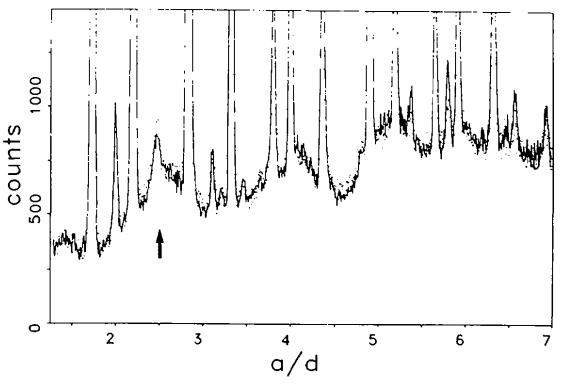

Fig. 5. Enlarged room-temperature (solid line) and 770 K (points) powder diagrams of CSZ showing the broad modulations of the background and the 'forbidden' 211_{cub} reflexion (arrow). To eliminate the temperature change of the lattice constants $a/d = (h^2 + k^2 + l^2)^{1/2}$ is given on the abscissa.

the extra peak indicates tetragonal short-range order (of a sublattice) within the strictly cubic matrix rather than an exsolved minority phase. The width of the 211 reflexion is compatible with correlation lengths of about 30 Å at r.t. and about 80 Å at 770 K for these tetragonal domains.

The possibility that cubic zirconia could indeed be regarded as a coherent intergrowth of small tetragonal domains was examined by refinements in the tetragonal space group $P4_2/nmc$ but with a strictly cubic metric. Three further models were therefore considered: refinements with harmonic B factors did not show any significant shift of O away from 0.5, *i.e.* this is identical to the cubic harmonic model in Table 2(*a*). However, an anharmonic third-order refinement showed a significant improvement of the fit (Table 2*b*; c^{223} was again not significant). The corresponding oxygen p.d.f. (Fig. 6*a*) shows extra density on interstitial positions along $\langle 00z \rangle$ in addition to the main p.d.f. peak, which is still located exactly(!) at the 'cubic' position ($z = 0.5$). Note that the refined positional parameter does not coincide with the maximum of the p.d.f. (*cf.* Boysen, 1992). Because of unphysically large negative p.d.f. regions, however, an interstitial-atom model was refined subsequently (Table 2*b*, Fig. 6*b*) and is therefore preferred in spite of worse R factors. To separate 'cubic' and 'tetragonal' parts, a distribution of 'cubic' ($z = 0.5$) and 'tetragonal' ($z \neq 0.5$) oxygen sites was introduced (O and O′, respectively, in Table 2). The total O occupation is less than in the cubic anharmonic model but still too large at r.t. and again reduces to the stoichiometric value at 770 K. The O′ atoms have a large B value of 7 (1) Å^2 and a Δz shift of 0.10 (1). These values strongly deviate from values $B(\mathrm{O}) = 0.7$ (1) Å^2 and $\Delta z(\mathrm{O}) = 0.05$ (1) for ordered tetragonal zirconia and indicate a pronounced disorder of these tetragonal regions.

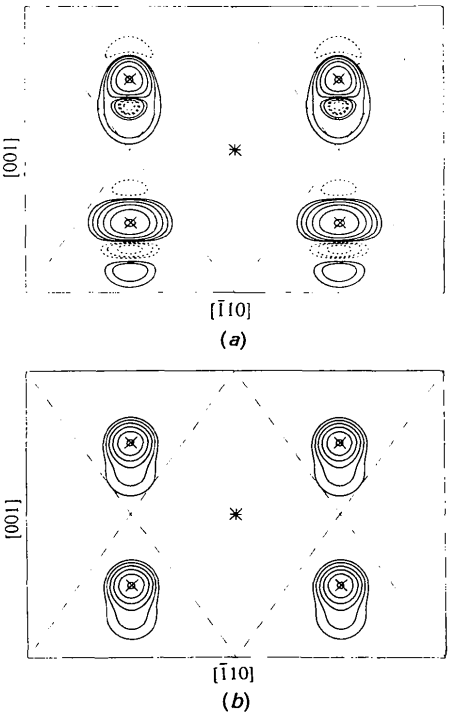

Fig. 6. Oxygen p.d.f. maps of CSZ at room temperature obtained from refinements in space group $P4_2/nmc$ with (*a*) anharmonic coefficients up to the third order and (*b*) oxygen interstitials at [00z]. Dashed lines indicate negative p.d.f. regions.

Table 3. *Decomposition of isotropic harmonic temperature factors (equivalent ones for TZP) into static and dynamic components at room temperature*

		B_{tot} (Å^2)	B_{stat} (Å^2)	B_{dyn} (Å^2)
O	CSZ	3.3 (1)	3.1 (4)	0.2 (4)
	TZP	0.7 (1)	0.2 (1)	0.5 (1)
Zr	CSZ	1.17 (6)	0.79 (6)	0.38 (6)
	TZP	0.37 (4)	0.05 (6)	0.32 (6)

In summary, the two fitting approaches yield similarly good fits. Note that the R factors cannot be compared directly owing to the different number of reflexions included, although the goodness of fit slightly favours the tetragonal approach. Both may be considered as approximations to the envisaged real situation: a strictly cubic latice with coherent distortions of the oxygen sublattice with correlation lengths between 30 and 70 Å. The unrealistically large n(O) may be a consequence of the fact that the real situation is not adequately described. New refinement procedures simultaneously including sharp and broadened Bragg reflexions and diffuse scattering have to be developed.

4. Discussion

A comparison of the average structure and the disorder in the two materials reveals large differences between the absolute values of the structural parameters and between their temperature dependences. These differences owe particularly to the considerably larger static disorder of the cubic phase (CSZ). After subtraction of the static Gaussian parts, the remaining dynamic parts of the thermal parameters at r.t. are given in Table 3. The large standard deviations for CSZ are arbitrary and take care of the problematic separation of static disorder. Clearly, the overall isotropic dynamic behaviour is quite similar in the two cases. There are, however, differences in the anisotropy, as may be seen not only from the second-order terms of the temperature factor but also from the third-order terms: if TZP behaved as though it were cubic, the conditions $c^{223} = -c^{113}$ and $c^{333} = 0$ should hold, which is not the case (*cf.* Table 1). Fig. 7 shows the significant anharmonic third-

order terms plotted as a function of T^2. Both coefficients show the expected linear increase above 770 K, whereas the deviations below this temperature in CSZ again have to be attributed to static contributions.

The differences in the dynamic behaviours in the two systems may best be discussed with the help of p.d.f. maps in the planes shown schematically in Fig. 8. It must be remembered that the p.d.f. maps of CSZ (Fig. 9) are strongly influenced by the static disorder. This is demonstrated again by the pronounced temperature variation of the pseudopotentials shown in Fig. 10(*a*), which contrasts with the behaviour of TZP, the potential of which is nearly independent of temperature (Fig. 10*b*). Although it is therefore difficult to extract the dynamic contributions in CSZ, some hints may be gained from the change of the form of the p.d.f. between r.t. and 770 K. At the higher temperature, bulges in the ⟨111⟩ directions have developed. Such bulges become even more pronounced at higher temperatures, as reported by Lorenz *et al.* (1988). They were interpreted as indications of the diffusion pathways of the anions: first along ⟨111⟩ through a face of the surrounding cation tetrahedron into the octahedral cavity (indicated by the asterisk in Fig. 9), then turning towards ⟨001⟩ and finally re-entering the nearest-neighbour cation site along ⟨111⟩.

The p.d.f. maps of TZP (Fig. 11) show similar bulges pointing towards the octahedral cavity in the equivalent section (Figs. 11*a* and 11*b*) but only in the lower part of the picture, while the bulges of the symmetrically equivalent atoms in the upper part point towards another octahedral cavity (obtained by application of the 4_2 symmetry axis). Therefore, a migration to the nearest-neighbour anion positions along the [001]$_t$ direction seems to be improbable. On the other hand, a pathway between next-nearest neighbours along [100]$_t$ or [010]$_t$ in the upper or lower oxygen layer, respectively, seems to be likely. In addition, migration by next-nearest-neighbour jumps between these layers is also possible but, as shown by Fig. 11(*c*), only between those pairs of atoms that approach each other because of the tetragonal distortion of the oxygen sublattice (*cf.* Fig. 8). Note that in the tetragonal structure the puckered oxygen layers may be subdivided into two sublayers each approaching different layers of octahedral cavities. Therefore, diffusion is restricted to planar slabs formed by the two sublayers nearest to

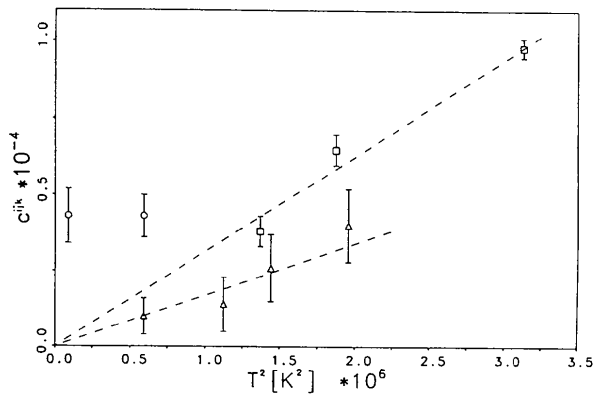

Fig. 7. Temperature dependence of the third-order anharmonic coefficients $-c^{113}$ of TZP (△) and c^{123} of CSZ (○, this work; □, Lorenz *et al.*, 1988).

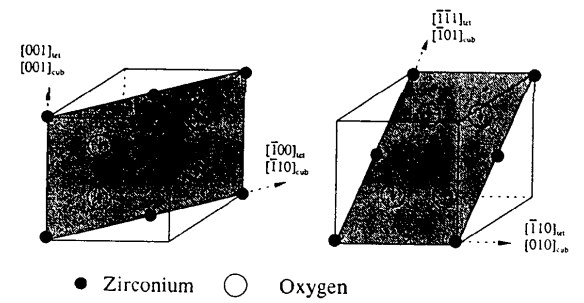

Fig. 8. Correspondence of lattice planes shown in the p.d.f. maps (Figs. 6, 9 and 11) in cubic and tetragonal notation. The arrows indicate the shifts of the oxygens in the tetragonal phase.

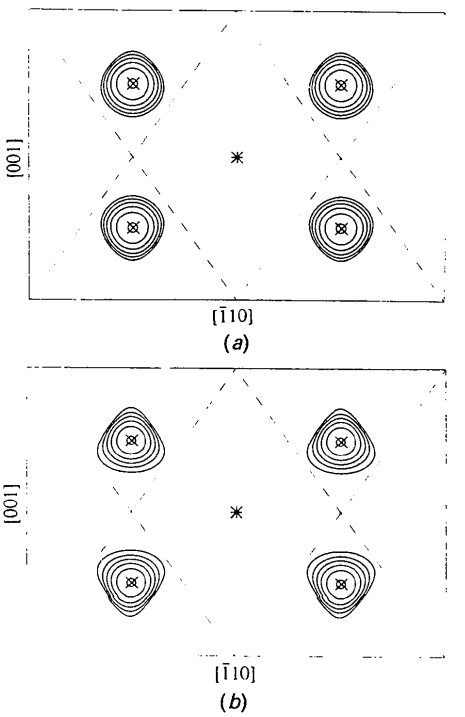

Fig. 9. Oxygen p.d.f. maps for CSZ at (*a*) room temperature and (*b*) 770 K corresponding to (both) sections shown in Fig. 8. Refinement in space group *Fm3m* with anharmonic terms up to the fourth order. Contour lines correspond to 3, 6, 12, 24, 48 and 96% of maximum. The dashed lines indicate the traces of the faces of the surrounding Zr tetrahedron, crosses mark the tetrahedral cavity, the asterisk the octahedral cavity.

the cavity layer. This contrasts with the behaviour in CSZ, where diffusion may take place in all $\langle 100\rangle_c$ directions (or $\langle 110\rangle_c$ directions at low temperatures?) with, however, larger jump distances than in TZP. Note that the p.d.f. in TZP 'touches' the face of the surrounding cation tetrahedron. Hence, the enhanced ionic conductivity in TZP may be at least partly related to a structural origin (see below). It has to be admitted, however, that definite conclusions about diffusion pathways can only be made by the direct observation of a continuous density in the p.d.f. maps. Then the potential barrier along the pathways can be compared with activation energies determined by conductivity measurements. In the present case the temperatures are not high enough to allow such a comparison, since the activation energy for TZP (3% Y_2O_3) is too high: 0.62 eV [Weppner & Schubert, 1988; *cf.* equation (2)].

Although the foregoing discussion suggests a partial influence of the structure itself, a probably more important reason for the reduced conductivity in CSZ is the considerably larger static disorder in this compound. At r.t. most of the O vacancies in CSZ are concentrated in microclusters embedded in the average cubic structure. These vacancies are then not available for the conduction process. There are, however, additional incoherent precipitations, which may be concluded from an increase of the scale factors by about 10% from r.t. to 770 K: this means that the amount of coherently scattering matter has increased. At the same time, the intensity of the diffuse background must decrease. As shown in Fig. 5 the background remains virtually unchanged, *i.e.* the decrease is roughly compensated by the normal increase due to thermal diffuse scattering (multiphonon background). Possibly, these incoherent precipitations have a larger vacancy concentration and, as anticipated before, in turn this could explain (part of?) the too large oxygen occupancy found at r.t. for

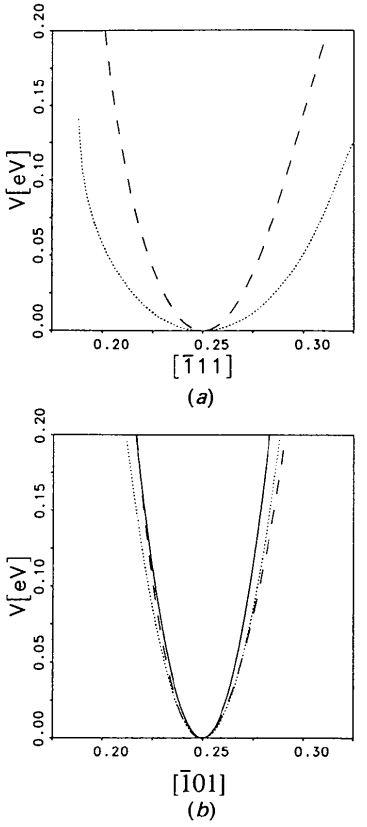

Fig. 10. Temperature dependence of the one-particle potentials of oxygen in (*a*) CSZ and (*b*) TZP. Dotted line, room temperature; dashed line, 770 K; solid line, 1400 K.

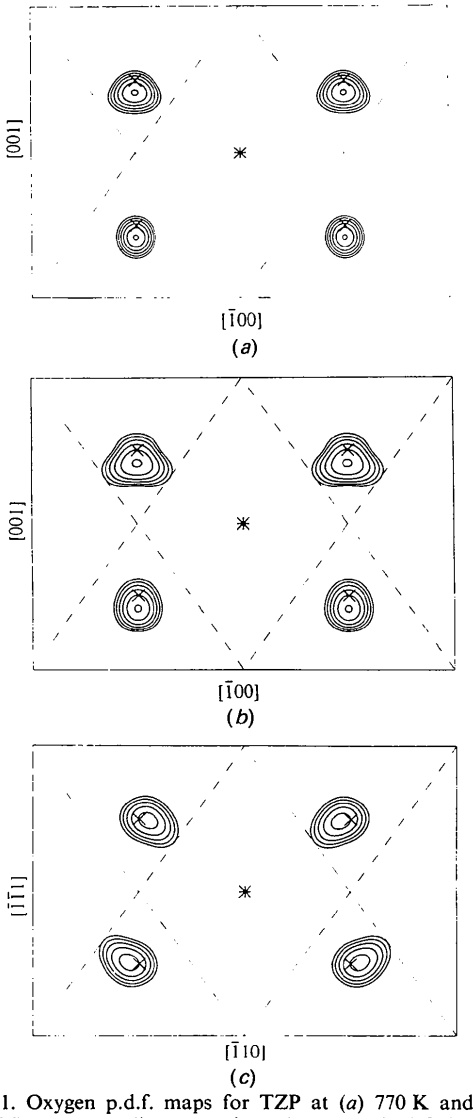

Fig. 11. Oxygen p.d.f. maps for TZP at (*a*) 770 K and (*b*), (*c*) 1400 K corresponding to sections shown on the left (*a*), (*b*) and right (*c*) in Fig. 8. Refinements in space group $P4_2/nmc$ with anharmonic third-order coefficients. Note that in (*c*) the O atoms do not lie exactly in the plane.

the average matrix structure. In any case, the microclusters seem to stabilize the overall cube lattice (by strains?) of the CSZ grains. This interpretation seems to be incompatible with the results of Neder *et al.* (1990), who concluded from the interpretation of the diffuse scattering of CSZ that there was coherent clustering around single and double vacancies. Note, however, that single crystals and powders of the same overall composition may exhibit remarkable structural differences, in particular different types of disorder. For example, the 'tetragonal' 211 reflexion is not present in the single crystal of even the same source. The coexistence of different types of domains (incoherent and coherent) is also discussed in the literature (Butler, Catlow & Fender, 1983; Osborn, Andersen, Clausen & Hackett, 1986). In consequence, it is not surprising that tetragonal domains found in CSZ powder are absent in single crystals. On the other hand, it cannot be completely excluded that part (but not all!) of the disorder in the powder evidenced by the diffuse background can be attributed to the same type of microclusters as in the single crystal or any other type, including Φ_1-like domains, as suggested by Rossel *et al.* (1991). A complete quantitative calculation of the modulated diffuse background, which could in principle be more decisive, is beyond the scope of this paper.

For several reasons the reordering process in CSZ seems to be continuous; it does not just occur abruptly at 1150 K, as might be suggested in Fig. 4: the increase of B(O) from r.t. to 770 K is unphysically small. An explanation is that the static part at 770 K is already smaller than that at r.t. or, in other words, the increase of dynamic disorder is compensated by a decrease of static disorder. The third-order coefficients of O remain constant for both temperatures; the fourth-order terms even decrease with temperature. This behaviour points to a general decrease of static disorder with temperature. Moreover, the decrease of the O occupancy from r.t. to 770 K is a consequence of the same ordering process. From these arguments we conclude that considerable ordering activities exist already in the temperature region below 1150 K.

Following these ideas we have to interpret the correct stoichiometric O occupation at 770 K as a disordering process where the clusters in CSZ gradually dissolve. At higher temperatures the vacancies are no longer fixed to their environment and become noticeable in the averaged structure by a more or less free motion through the structure. This discussion is also plausible from the thermodynamical point of view: at higher temperatures the O vacancies are no longer the decisive stabilizing factor for the (averaged) cubic structure because the stablity field of the true thermodynamically stable cubic phase is approached. This interpretation is compatible with results from recent diffuse-scattering experiments on single crystals (Proffen *et al.*, 1993), which show that the diffuse scattering decreases at approximately the temperature at which the bend in the temperature dependence of B(O) was observed here. Although it has to be kept in mind that the behaviour of single crystals and powders is obviously different, the stability field of the cubic phase is still approached. From the phase diagram of ZrO_2–Y_2O_3 one could expect a similar behaviour in TZP. This has not been found, *i.e.* the tetragonal phase does not form correlated microclusters for its stabilization. This may be understood, since the lower concentration of vacancies in TZP (larger distances between defects) does not lead to correlations between the defects.

In conclusion, the enhanced low-temperature conductivity of TZP in spite of a lower vacancy concentration as compared to CSZ is partly due to a more favourable arrangement in the average structure but mostly to the immobilization of vacancies in CSZ by clustering. Finally, microstructural aspects like diffusion along grain boundaries, which could not be analysed in the present work, could play an additional role in the better ionic conductivity of TZP.

We thank P. Kountouros and Dr H. Schubert, MPI f. Metallforschung, Stuttgart, for providing the TZP samples. Thanks are also due to the Deutsche Forschungsgemeinschaft for supporting this investigation under Fr 747/1.

References

BACHMANN, R. & SCHULZ, H. (1984). *Acta Cryst.* A**40**, 668–675.
BONANOS, N., SLOTWINSKI, R., STEELE, B. & BUTLER, B. (1984). *J. Mater. Sci.* **19**, 785–793.
BOYSEN, H. (1992). *Accuracy in Powder Diffraction* II, *Proceedings*, edited by E. PRINCE & J. STALICK, pp. 165–174. Gaithersburg: National Institute of Standards and Technology.
BOYSEN, H., FREY, F. & VOGT, T. (1991). *Acta Cryst.* B**47**, 881–886.
BUTLER, V., CATLOW, C. & FENDER, B. (1983). *Radiat. Eff.* **73**, 272–277.
CARTER, R. & ROTH, W. (1968). *Electromotive Force Measurements in High Temperature Systems*, edited by C. B. ALCOCK, pp. 125–144. London: Institute of Mining and Metallurgy.
FABER, J., MÜLLER, M. & COOPER, B. (1978). *Phys. Rev. B*, **17**, 4884–4888.
FREY, F., BOYSEN, H. & VOGT, T. (1990). *Acta Cryst.* B**46**, 724–730.
HOWARD, C. J., HILL, R. J. & REICHERT, B. E. (1988). *Acta Cryst.* B**44**, 116–120.
JOHNSON, C. K. & LEVY, H. A. (1974). *International Tables for X-ray Crystallography*, Vol. IV, pp. 311–336. Birmingham: Kynoch Press. (Present distributor Kluwer Academic Publishers, Dordrecht.)
KUHS, W. (1992). *Acta Cryst.* A**48**, 80–98.
LORENZ, G., FREY, F., SCHULZ, H. & BOYSEN, H. (1988). *Solid State Ionics*, **28–30**, 497–502.
MARXREITER, J. (1989). Thesis, Univ. of Munich, Germany.
MICHEL, D., MAZEROLLES, L. & PEREZ Y JORBA, M. (1983). *J. Mater. Sci.* **18**, 2618–2628.

MITSUHASHI, T., ICHIHARA, M. & TATSUKE, U. (1974). *J. Am. Ceram. Soc.* **57**, 97–101.
MORINAGA, M., COHEN, J. B. & FABER, J. (1979). *Acta Cryst.* A**35**, 789–795.
NEDER, R. B., FREY, F. & SCHULZ, H. (1990). *Acta Cryst.* A**46**, 799–809.
NETTLESHIP, I. & STEVENS, R. (1987). *Int. J. High Tech. Ceram.* **3**, 1–32.
OSBORN, R., ANDERSEN, N. H., CLAUSEN, K. & HACKETT, M. A. (1986). *Mater. Sci. Forum*, **7**, 55–62.
PROFFEN, T., NEDER, R. B., FREY, F., KEEN, D. A. & ZEYEN, C. M. E. (1993). *Acta Cryst.* B**49**. In the press.
ROSSEL, H. J., SELLAR, J. R. & WILSON, I. J. (1991). *Acta Cryst.* B**47**, 862–870.
SCOTT, H. G. (1975). *J. Mater. Sci.* **10**, 1527–1535.
STUBICAN, V. S. (1988). *Adv. Ceram.* **24**, 71–82.
TEUFER, G. (1962). *Acta Cryst.* **15**, 1187.
THOMAS, A. & BENDALL, P. J. (1978). *Acta Cryst.* A**34**, S-351.
TURRILLAS, X., SELLARS, A. P. & STEELE, B. C. H. (1988). *Solid State Ionics*, **28–30**, 465–469.
WEPPNER, W. & SCHUBERT, H. (1988). *Adv. Ceram.* **24**, 837–843.
ZUCKER, U. H., PERENTHALER, E., KUHS, W. F., BACHMANN, R. & SCHULZ, H. (1983). *J. Appl. Cryst.* **16**, 358.

Acta Cryst. (1993). B**49**, 413–420

Structure Determination from Small Crystals of Two Aluminophosphates, CrAPO-14 and SAPO-43

BY MADELEINE HELLIWELL

Department of Chemistry, University of Manchester, Manchester M13 9PL, England

VENCESLAV KAUČIČ

Department of Chemistry and Chemical Technology, University of Ljubljana, 61000 Ljubljana, Slovenia, and Boris Kidrič Institute of Chemistry, 61000 Ljubljana, Slovenia

AND G. M. T. CHEETHAM, MARJORIE M. HARDING, B. M. KARIUKI AND P. J. RIZKALLAH

Chemistry Department, Liverpool University, PO Box 147, Liverpool L69 3BX, England

(*Received* 10 *March* 1992; *accepted* 21 *August* 1992)

Abstract

Small single crystals, *ca* 10^5 μm^3, of two aluminophosphates have been used to determine their structures. Both compounds were synthesized with the aim of incorporating chromium into the framework, and for CrAPO-14 the X-ray diffraction results show that this has been achieved. For CrAPO-14, $Al_{3.96}Cr_{0.04}(PO_4)_4(OH).C_3H_{10}N.H_2O$, data recorded on a Rigaku AFC-5R diffractometer (Cu $K\alpha$) and, independently, on an Enraf–Nonius FAST diffractometer (Mo $K\alpha$), showed the structure to be like that of GaPO-14 [Parise (1986). *Acta Cryst.* C**42**, 670–673]; aluminium atoms occupy four-, five- and six-coordinated sites, and 4–5% of the aluminium in the six-coordinate site is replaced by chromium. For SAPO-43, $Al_2(PO_4)_2(C_3H_{10}N)$, data were recorded independently on the AFC-5R (Cu $K\alpha$) and on a FAST diffractometer with synchrotron radiation of wavelength 0.895 Å; the structure is like that of gismondine [Alberti & Vezzalini (1979). *Acta Cryst.* B**35**, 2866–2869], but replacement of Al by Cr to a significant extent could not be established. Framework Al, P and O atoms are located with e.s.d.'s of 0.001–0.005 Å, template atoms with e.s.d.'s of *ca* 0.01 Å in CrAPO-14, and larger e.s.d.'s in SAPO-43 where there is disorder in the template-molecule position. In all these respects the two independent determinations for each structure are in agreement. The effectiveness of the different methods of intensity-data collection is compared.

Introduction

The synthesis and characterization of aluminophosphates and related materials with catalytic properties provide considerable challenges. In the synthetic program at Ljubljana University, materials prepared include aluminophosphates (ALPO's), with compositions $Al_2O_3.P_2O_5.xR.yH_2O$ where R is a template molecule (usually an amine), and further aluminophosphates in which some aluminium and sometimes also phosphorus is replaced by silicon, known as SAPO's; in other materials small amounts of metals, usually transition metals, replace aluminium or phosphorus. These chemical variations lead to a wide range of structure types; some can be related to zeolite structure types and others are new (Flanigen, Lok, Patton & Wilson, 1986; Bennett & Marcus, 1988; Rajić, Kaučič & Stojaković, 1990; Nardini,

0108-7681/93/030413-08$06.00